Dynamic gating window for compensation of baseline shift in respiratory-gated radiation therapy

Eric W. Pepin[a)]
School of Health Sciences, Purdue University, West Lafayette, Indiana 47907

Huanmei Wu
Purdue School of Engineering Technology, IUPUI, Indianapolis, Indiana 46202

Hiroki Shirato
Hokkaido University School of Medicine, Sapporo, Japan 060-8638

(Received 19 October 2010; revised 20 January 2011; accepted for publication 29 January 2011; published 11 March 2011)

Purpose: To analyze and evaluate the necessity and use of dynamic gating techniques for compensation of baseline shift during respiratory-gated radiation therapy of lung tumors.
Methods: Motion tracking data from 30 lung tumors over 592 treatment fractions were analyzed for baseline shift. The finite state model (FSM) was used to identify the end-of-exhale (EOE) breathing phase throughout each treatment fraction. Using duty cycle as an evaluation metric, several methods of end-of-exhale dynamic gating were compared: An *a posteriori* ideal gating window, a predictive trend-line-based gating window, and a predictive weighted point-based gating window. These methods were evaluated for each of several gating window types: Superior/inferior (SI) gating, anterior/posterior beam, lateral beam, and 3D gating.
Results: In the absence of dynamic gating techniques, SI gating gave a 39.6% duty cycle. The ideal SI gating window yielded a 41.5% duty cycle. The weight-based method of dynamic SI gating yielded a duty cycle of 36.2%. The trend-line-based method yielded a duty cycle of 34.0%.
Conclusions: Dynamic gating was not broadly beneficial due to a breakdown of the FSM's ability to identify the EOE phase. When the EOE phase was well defined, dynamic gating showed an improvement over static-window gating. © *2011 American Association of Physicists in Medicine.* [DOI: 10.1118/1.3556588]

Key words: lung cancer, respiratory motion, respiratory gating, baseline shift

I. INTRODUCTION

It has been well documented that respiratory motion creates an uncertainty in the targeting of radiotherapy for lung tumors[1] and that this motion can be greater than 1–5 cm,[2–7] though smaller in medial and apical tumors.[8] This uncertainty brings about a need for larger treatment margins in conventional radiation therapy,[6] usually 1–2 cm (Refs. 9 and 10) and as high has 3.1 cm.[11] Respiratory gating is an advanced image guided radiation treatment approach to compensate tumor motion induced by patient respiration. The beam is on only when the tumor is in a certain predefined region, i.e., *the gating window*. Gating has been in use since the late 1980s.[12,13] Its primary application is for lung cancer, but applications have included liver[7] and breast cancer.[14] Previous studies have shown that respiratory gating can reduce treatment margin up to 36% in the superior/inferior (SI) direction, giving margins as small as 3 mm.[4,11,15–17] However, respiratory gating increases the total treatment time of a patient.[18]

Based on gating window determination, there are two common gating approaches: Phase-based gating and amplitude gating. In phase-based gating, the gating window is set to be some percent of the breathing cycle, effectively fixing the duty cycle.[19] In amplitude-based gating, the window is a fixed width about some window center corresponding to tumor motion in the SI, lateral (LAT), and/or anterior/posterior (AP) directions.[18–21] Studies have been done with gating windows ranging from 2.5 to 12.5 mm wide[18] and by defining the window based on displacement percentiles.[21] One study showed little difference between phase-based and amplitude-based gating.[19] Gating windows are often defined about the most extreme positions in the breathing cycle:[9] The end-of-exhalation (EOE) and the end-of-inhalation (EOI). EOE is chosen more often[7,10,15–17,20,22–24] and is more effective[4] because EOE has longer duration and slower tumor motion.[8,9,16,25] In addition, the position of the EOE window is more reproducible.[3,19,20,25,26] EOI gating is often used with a breath-hold technique (deep-inspiration breath-hold) to increase reproducibility and stability.[5,26,27] EOI gating has the advantage of lower lung toxicity to surrounding normal tissue than EOE gating;[2,8,9,19,25,26] however, EOI gating has more residual motion than EOE gating.[19]

One metric for evaluating respiratory gating is the duty cycle, which is the fraction of total treatment time during which radiation is being delivered. In fixed-duty cycle experiments, the efficacy of duty cycles ranging from 20% to 50% have been studied.[1,9,11,15,21,22,24,26–28] In experiments with fixed gating windows, duty cycles ranging from 12.2% to 69% have been seen.[4,7,8,17,20] Various studies have sought to improve the performance of respiratory gating by provid-

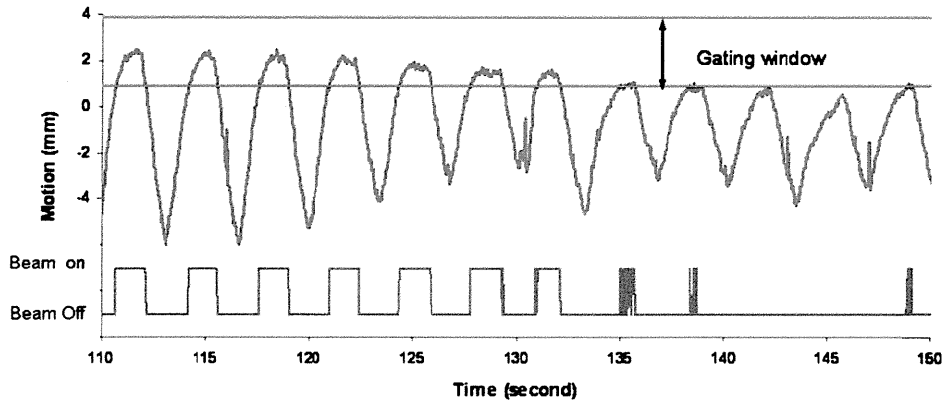

FIG. 1. Fixed amplitude-based gating window for tumor motion with baseline shift and the corresponding beam on/off signal over time.

ing audio or visual coaching to patients so as to increase the reproducibility and stability of their breathing patterns, especially while the tumor is in the gating window.[3,7,9] It has been found that EOI gating with audio coaching is equivalent to EOE gating when both techniques have a fixed 30% duty cycle.[19]

Respiratory motion is patient-specific and there are changes over time in motion amplitude, respiratory period, and baseline location from one breathing cycle to another. In addition, there is noise signal, including random spike noise generated from the tracking system and noise from cardiac motion.[29] Figure 1 illustrates the superior-inferior motion trace of a lung tumor tracked based on an internal implanted fiducial marker. Phase-based gating is vulnerable to duty cycle fluctuations and amplitude variation, which will decrease the effectiveness of the treatment and potentially increase false beam on time, such as during 135–150 s in Fig. 1. In a phase-based gating scenario, the beam will be on even though the tumor is not in the gating window. The amplitude-based gating can detect the motion changes; however, the gating duty cycle will be low and will result in much longer treatment time, especially with baseline shift, as demonstrated in Fig. 1. In addition, noise in the motion signal can cause frequent beam toggling, especially if the gating window is not appropriately set, as shown in the latter portion of Fig. 1.

It has been recommended to account for baseline shift when respiratory gating, i.e., a dynamic window center.[14] However, only limited work has been done to improve duty cycles by adjusting the gating window.[20] In this work, we present several methods of dynamic gating for real-time baseline shift compensation and an analysis of their efficacy.

II. METHODS AND MATERIALS

II.A. Materials

This study used the 3D motion of implanted gold fiducials in 30 lung tumors during 592 radiotherapy fractions tracked using real-time fluoroscopy at a rate of 30 Hz by Hokkaido University.[30] Tumor fiducials were tracked with four orthogonal fluoroscopes during individual treatment fractions, generating tuples of the form (t,x,y,z), where x is LAT position, y is SI position, and z is AP position. The average amplitude of tumor motion for each treatment fraction in three dimensions was 13.9 mm (σ=8.2) and the average baseline drift was 6.6 mm (σ=9.2) in the LAT direction, 9.6 mm (σ=10.3) in the SI direction, and 9.1 mm (σ=11.8) in the AP direction. The tumors are considered as solid and nondeformable tumors. If only translational motion is considered, the motion trajectory represents the motion of each voxel in the tumor and the GTV motion.

II.B. Methods

II.B.1. Motion data preprocessing

The motion data were classified using the finite state model (FSM) developed by Wu.[31] The FSM is a real-time algorithm for classifying the breathing state of a motion data point from a moving lung tumor. In the FSM, a data point is classified in one of four breathing states: Exhale, EOE, inhale, and irregular.

II.B.2. Gating window definition

The size of the gating window can be determined in different ways. A smaller gating window will reduce radiation dose to surrounding healthy tissue and critical structures, yet result in lower gating duty cycle, longer treatment duration, and more beam on/off changes. A larger gating window would result in higher duty cycle, yet increased treatment margins. In practice, the gating window size is decided based on the patient-specific respiratory motion patterns and depends on motion stabilities, amplitude, tumor volume, and other information. For this study, gating window sizes of 3 and 5 mm are simulated and compared. A fixed gating window was defined as a 3 or 5 mm spatial window centered on the average tumor position during one or more complete EOE phases, as the EOE state has relative small motion. Four different gating windows were investigated.

- Gating window based on SI position: The gating window was a 1.5 or 2.5 mm expansion for the 3 or 5 mm

gating window, respectively, in each of the superior/inferior directions about the average position of the tumor in the EOE phase.

- Gating window based on AP beam: The gating window was a 1.5 or 2.5 mm expansion in each direction perpendicular to an AP beam, i.e., superior, inferior, right, and left.
- Gating window based on LAT beam: The gating window was a 1.5 or 2.5 mm expansion in each direction perpendicular to a LAT beam, i.e., superior, inferior, anterior, and posterior.
- Gating window based on 3D position: The gating window was a 1.5 or 2.5 mm expansion in each anatomic direction, i.e., superior, inferior, right, left, anterior, and posterior.

II.B.3. Gating window position determination

Three different methods were used to determine how to center the gating window.

- The static gating window center was the average tumor position during the first three EOE phases of the treatment fraction.
- The ideal gating window had gating windows determined *a posteriori* for each EOE phase and placed on the center of each EOE phase.
- Several types of dynamic gating windows had the center of the window changed upon leaving each EOE phase.

II.B.4. Dynamic gating algorithms

Two methods of changing the gating window center were evaluated.

- In the weighted-center method, the average tumor position for each of the previous three EOE phases was considered as the vector triples (x_1,y_1,z_1), (x_2,y_2,z_2), and (x_3,y_3,z_3). The window center was calculated as a weighted average of the vector triples

$$w_1(x_1,y_1,z_1)+w_2(x_2,y_2,z_2)+w_3(x_3,y_3,z_3)$$

where $0\leq w_i\leq 1$, $w_1+w_2+w_3=1$, and $w_1=n\cdot 0.05, n\in Z_{20}$.

All combinations of w_1, w_2, and w_3 were considered and the duty cycle for each combination was calculated for each treatment fraction. For each fraction, the weighting combinations giving the ten largest duty cycles were recorded. Three-dimensional histograms were made showing the number of times each weighting combination was considered favorable using scatter3 in MATLAB (MATLAB® The MathWorks, Natick, MA).

- In the trend-line method, the gating window center was calculated using the slope of a linear regression line fit to the average tumor position of each of several previous EOE phases. This method was evaluated considering the previous two, three, four, and five EOE phases. The window center was calculated by extending the trend-line from its calculated path. N.B.: The trend-line method for three previous EOE phases is a special case of the weighted-center method in which $w_1=w_2=w_3$.

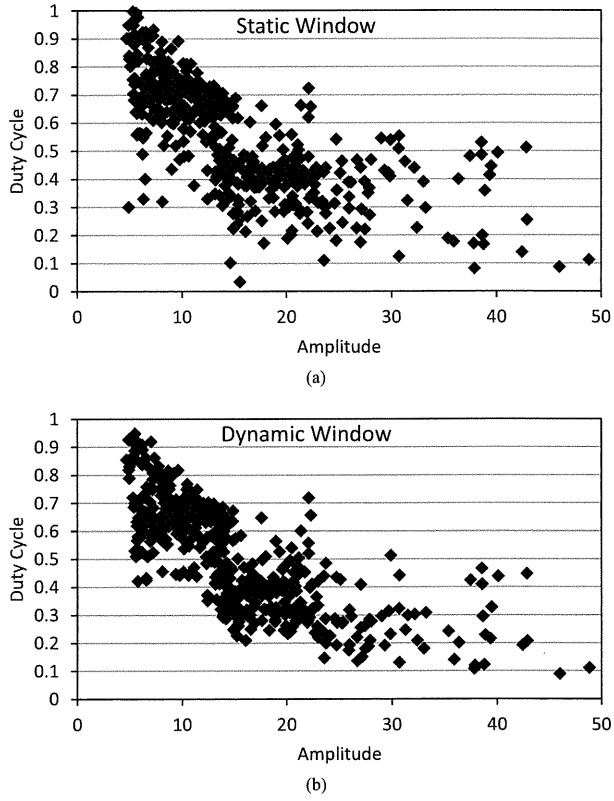

FIG. 2. The relationships of duty cycle and amplitude for each fraction of (a) static gating and (b) dynamic gating, where the gating window size is 5 mm

For each gating window method, the duty cycle was calculated as the fraction of total tracking time that the tumor was located within the gating window.

III. RESULTS

For a 3 mm gating window size, the static-window gating method gave an average duty cycle of 39.6% (σ=17.6%) for a SI gate. The ideal-window gating method gave a significantly larger average duty cycle of 41.5% (σ=16.0%) for a SI gate ($p<0.001$). For the 3D window, the average duty cycle improvement was 4.3% when comparing the ideal window to the static window. Similarly, this improvement was 2.6% for the AP beam and 4.0% for the LAT beam. The analysis was repeated with a 5 mm gating window, the comparative results were unchanged, with duty cycles being increased 12%–14% in all cases. The relationships between the duty cycle and the amplitude (averaged over a treatment fraction) are compared and illustrated in Fig. 2. The scattered plots showed that for fractions with small amplitude and/or low duty cycle, there is more increase of duty cycle from static gating to dynamic gating. This effect was more pronounced with the 5 mm gating window.

The remaining results are presented based on the 3 mm gating window. The weight-based method of dynamic gating

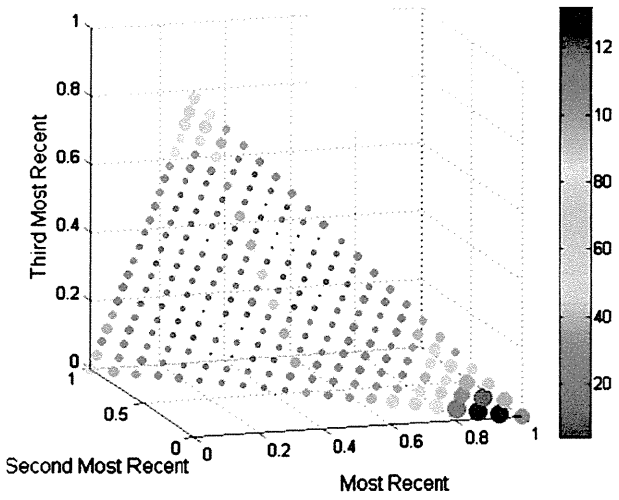

FIG. 3. Histogram showing favorability of weighting combinations for a gating window determined only by considering SI position. The size/color of each marker indicates the favorability of that combination. The histograms for AP, LAT, and 3D beams were similar.

performed best when the most recent EOE phase was given a weighting of at least 0.85 (see Fig. 3). Each fraction was evaluated for all weighting combinations in which w_1 was at least 0.85. The average duty cycle for all fractions shows little variability over the set of weighting combinations for a SI window (36.0%, σ=0.3%). It was also determined how many fractions, at each weighting combination, had duty cycles greater than the static-window case. For a SI gating window, these combinations produced a higher duty cycle in 25%–28% of fractions, with the most benefit occurring with the weighting combination $\langle 0.9, 0.05, 0.05\rangle$: 29%–33% of fractions saw benefits for an AP gating window, with the most benefit from $\langle 0.95, 0.05, 0\rangle$; 34%–39% of fractions saw benefits for a LAT gating window, with the most benefit from $\langle 0.95, 0.05, 0\rangle$; and 35%–40% of fractions saw benefits for a 3D gating window, with the most benefit from $\langle 0.95, 0.05, 0\rangle$.

The trend-line method of dynamic gating showed increasing duty cycle with more EOE phase averages considered in the trend-line from two to four (see Fig. 4). This increase was significant when comparing four EOE phase averages in the trend-line compared to only two for all gating window types ($p<0.03$). Including five EOE phases gave slightly lower duty cycles when compared to four EOE phases; however, this decline was not significant ($p>0.9$).

TABLE I. Comparison of duty cycles for each type of gating window and method of gating. The duty cycles given for the weighted window are those for the highest performing weighting combination for each window type.

Method	SI DC (%)	AP DC (%)	LAT DC (%)	3D DC (%)
Static window	39.6	36.0	31.0	29.3
Ideal window	41.5	38.6	35.0	33.6
Weighted window	36.2	33.3	29.4	28.1
Trend-line window (n=4)	34.0	30.1	26.6	25.1

The results for all methods and window types are summarized in Table I.

IV. DISCUSSION

It was somewhat unexpected that the overall performance over the 30 patients of the real-time dynamic gating methods did not outperform a static window. This led to an investigation of individual tumors and whether a particular gating method consistently produced an increase in the duty cycle during the treatment of particular tumors. The investigation found that tumor motion behavior and motion patterns have great influence on the gating duty cycle. Not all 30 tumors exhibited a significant baseline shift over time and as such, the advantage of dynamic gating did not show. In practice, it may be beneficial to consider the amplitude of tumor motion when fixing the width of the gating window.

For some tumors' motion traces, there are distinctive changes in behavior between the IN, EX, and EOE states. The FSM can easily identify the unambiguous EOE phases as they are distinct from the other breathing phases (Fig. 5). Baseline shift in these motion patterns will benefit more from dynamic gating, as shown in Fig. 6. However, for some tumors, their motion trajectories do not have a prominent EOE stage, resulting in a motion trace that consists of IN and EX states, as shown in Fig. 7. Tumors with this type of motion are not suitable for gated treatment in the first place as it will lead to low duty cycle. In addition, the EOE state of the FSM

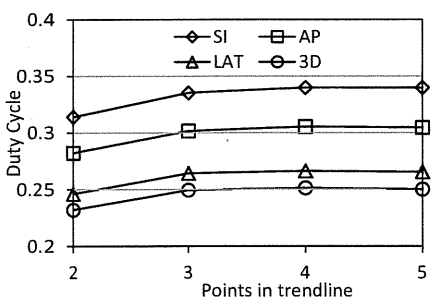

FIG. 4. Average duty cycle for trend-line-based dynamic gating for each window type and number of points in the trend-line.

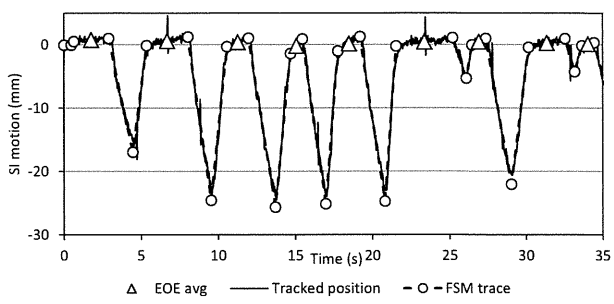

FIG. 5. Example of breathing pattern with well differentiated FSM transitions.

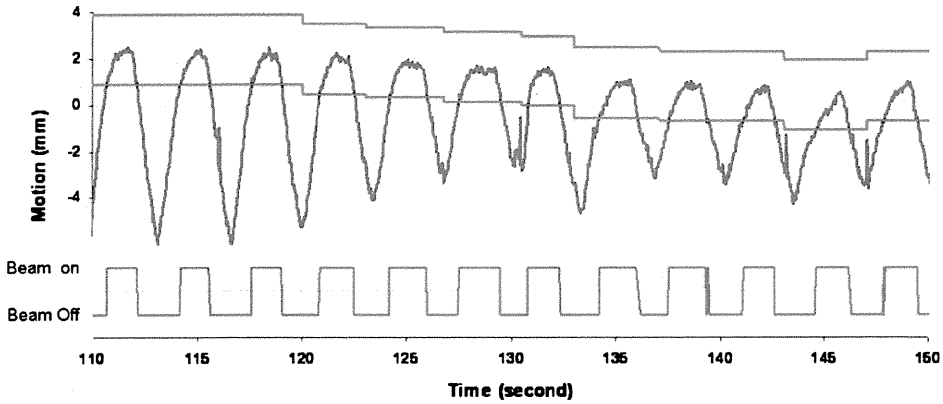

FIG. 6. This figure shows an amplitude-based ideal dynamic gating window being adjusted over the course of treatment.

model is highly variable. The gating window position of the dynamic gating approach is inconsistent for this type motion and the duty cycle is greatly affected.

Other than the duty cycle, several qualitative benefits were observed in the use of dynamic gating. In many of the fractions for which no duty cycle improvement was obtained, the EOE peak exited the static gating window, whereas with a dynamic window, the EOE peak was contained in the window. Two issues are masked by this apparent improvement in duty cycle. First, with the EOE peak exiting the gating window, a treatment interruption would be called for. However, this would likely be less than 2 s in duration, which is not achievable on most treatment machines. For the patient shown in Fig. 7, the instances of beam toggling are doubled for a fixed static window compared to the ideal dynamic window.

Another advantage of dynamic gating is shown in Fig. 8. The fixed gating window will require beam toggling nine times within three breathing cycles. Some of the beam toggles occur within 100 ms. The corresponding ideal dynamic window will only require three instances of beam toggling. For these three breathing cycles, the gating duty cycle changes from 34.4% to 47.7%.

Due to the noise in the motion signal and irregular breathing patterns, even with the ideal dynamic gating window, the amount of beam toggling is still substantial. A smoothing algorithm can be applied to avoid beam toggling caused by the noise signal. However, the beam toggling caused by irregular breathing patterns will not be solved by any smoothing algorithm. Additionally, it may be efficacious to recognize the location of the current EOE phase as it begins, rather than attempt to predict it *a priori*. The online FSM is able to do this with very short latency and modification of the online FSM for dynamic gating is another research direction for the presented work. At present, this is not feasible due to FSM

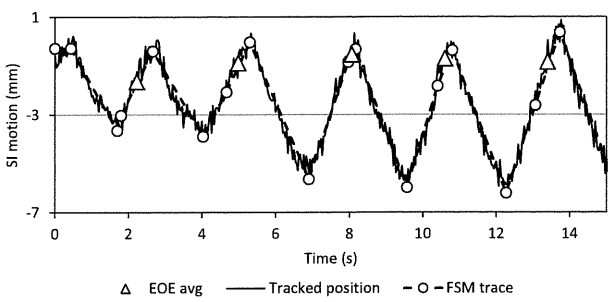

FIG. 7. Example of breathing pattern with poorly differentiated FSM transitions.

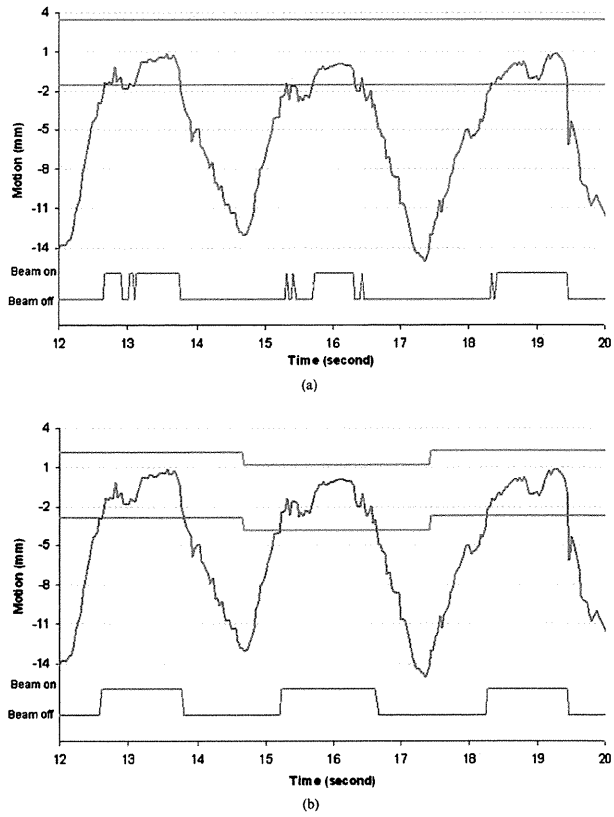

FIG. 8. Comparison of static and dynamic window showing scenario in which (a) static gating window requires additional rapid beam toggling and (b) the dynamic gating window perform better with less beam toggling and increased duty cycle. The gating window size is 5 mm in these two figures.

and mechanical system latencies, meaning that by the time the EOE phase is recognized and adjustments are made, it may already be over. A compromise could be informing the predicted location with a temporally closer phase, such as the immediately prior inhalation or exhalation phase.

Moreover, an interruption of the gating signal in the EOE phase is opposite the goals of EOE-based gating. The stability of the EOE phase is the reason for choosing it as the gating window and while a larger gating window that includes parts of the inhalation and exhalation phases might give a higher duty cycle, as sometimes occurs in the case of Fig. 7, the tumor would be in continuous motion while occupying that gating window. This trade-off of increased duty cycle for an unstable target would be clinically unacceptable. This suggests that further research is needed in placing the gating window in relation to the EOE phase and breathing phase transition points in order to minimize tumor motion within the gating window.

An additional factor that must be considered with the implementation of real-time treatment adjustments is how to redirect the radiation beam. In order to change the location of the gating window, either the patient must be moved through a treatment couch adjustment, or the radiation beam must be adjusted, possibly using a dynamic multileaf collimator. A side effect of such adjustments could be that while dose to the tumor is maintained, an increase in dose to surrounding normal tissue is introduced. Patient-specific limitations and boundaries would need to be determined *a priori* to ensure that the dose to critical structures is acceptable and quantifiable. Potential dose to normal tissue could possibly be quantified by overlaying the treatment plan on 4DCT images showing an anticipated adjusted anatomical state, i.e., temporally near the intended treatment phase. Such research and development is beyond the scope of this article, which will be investigated more in our ongoing research.

V. CONCLUSION

This paper proposed a dynamic gating approach to address the baseline shift problem caused by patient respiratory motion. Two methods of determining a dynamic gating window positions have been presented and analyzed. While dynamic gating did not guarantee an increased duty cycle for every patient, certain tumor locations and breathing motion patterns can see an increased duty cycle when dynamic gating is used. With duty cycle being just one factor in evaluating the efficacy of gated treatment, future research into the dosimetric implications of dynamic gating help determine if it is an attractive option for increasing the efficiency of respiratory-gated radiation therapy. Other qualitative considerations such as decreased beam toggling and increase tumor positional stability enhance the attractiveness of dynamic gating methods and require more research to quantify.

[a]Electronic mail: epepin@purdue.edu

[1]R. Li, J. H. Lewis, L. Cerviño, and S. B. Jiang, "A feasibility study of markerless fluoroscopic gating for lung cancer radiotherapy using 4DCT templates," Phys. Med. Biol. **54**, N489–N500 (2009).

[2]L. E. Butler *et al.*, "Dosimetric benefits of respiratory gating: A preliminary study," J. Appl. Clin. Med. Phys. **5**, 16–24 (2004).

[3]S. I. Denissova, M. H. Yewondwossen, J. W. Andrew, M. E. Hale, C. H. Murphy, and S. R. Purcell, "A gated deep inspiration breath-hold radiation therapy technique using a linear position transducer," J. Appl. Clin. Med. Phys. **6**, 61–70 (2005).

[4]M. Guckenberger *et al.*, "Potential of image-guidance, gating and real-time tracking to improve accuracy in pulmonary stereotactive body radiotherapy," Radiother. Oncol. **91**, 288–295 (2009).

[5]S. S. Korreman, T. Juhler-Nøttrup, and A. Boyer, "Respiratory gated-beam delivery cannot facilitate margin reduction, unless combined with respiratory correlated image guidance," Radiother. Oncol. **86**, 61–68 (2008).

[6]N. Linthout *et al.*, "Treatment delivery of time optimization of respiratory gated radiation therapy by application of audio-visual feedback," Radiother. Oncol. **91**, 330–335 (2009).

[7]E. Yorke, K. E. Rosenzweig, R. Wagman, and G. S. Mageras, "Interfractional anatomic variation in patients treated with respiration-gates radiotherapy," J. Appl. Clin. Med. Phys. **6**, 19–32 (2005).

[8]E. C. Ford, G. S. Mageras, E. Yorke, K. E. Rosenzweig, R. Wagman, and C. C. Ling, "Evaluation of respiratory movement during gated radiotherapy using film and electronic portal imaging," Int. J. Radiat. Oncol., Biol., Phys. **52**, 522–531 (2002).

[9]R. Muirhead, C. Featherstone, A. Diffton, K. Moore, and S. McNee, "The potential clinical benefit of respiratory gated radiotherapy (RGRT) in non-small cell lung cancer (NSCLC)," Radiother. Oncol. **95**, 172–177 (2010).

[10]A. Tai, J. D. Christensen, E. Gore, A. Khamene, T. Boettiger, and X. A. Li, "Gated treatment delivery verification with on-line megavoltage fluoroscopy," Int. J. Radiat. Oncol., Biol., Phys. **76**, 1592–1598 (2010).

[11]C. Nelson *et al.*, "Evaluation of tumor position and PTV margins using image guidance and respiratory gating," Int. J. Radiat. Oncol., Biol., Phys. **76**, 1578–1585 (2010).

[12]K. Ohara *et al.*, "Irradiation synchronized with respiration gate," Int. J. Radiat. Oncol., Biol., Phys. **17**, 853–857 (1989).

[13]C. G. Willett *et al.*, "The effect of the respiratory cycle on mediastinal and lung dimensions in Hodgkin's disease," Cancer **60**, 1232–1237 (1987).

[14]S. S. Korreman, A. N. Pedersen, T. J. Nøttrup, L. Specht, and H. Nyström, "Breathing adapted radiotherapy for breast cancer: Comparison of free breathing gating with the breath-hold technique," Radiother. Oncol. **76**, 311–318 (2005).

[15]H. H. Liu *et al.*, "Evaluation of internal lung motion for respiratory-gated radiotherapy using MRI: Part II—Margin reduction of internal target volume," Int. J. Radiat. Oncol., Biol., Phys. **60**, 1473–1483 (2004).

[16]S. Minohara, T. Kanai, M. Endo, K. Noda, and M. Kanazawa, "Respiratory gated irradiation system for heavy-ion radiotherapy," Int. J. Radiat. Oncol., Biol., Phys. **47**, 1097–103 (2000).

[17]R. W. M. Underberg, J. R. can Sörnsen de Koste, F. J. Lagerwaard, A. Vincent, B. J. Slotman, and S. Senan, "A dosimetric analysis of respiration-gated radiotherapy in patients with stage III lung cancer," Radiat. Oncol. **1**, 8–8 (2006).

[18]L. Dietrich, T. Tücking, S. Nill, and U. Oelfke, "Compensation for respiratory motion by gated radiotherapy: An experimental study," Phys. Med. Biol. **50**, 2405–2414 (2005).

[19]R. I. Berbeco, S. Nishioka, H. Shirato, and S. B. Jiang, "Residual motion of lung tumors in end-of-exhale respiratory gated radiotherapy based on external surrogates," Med. Phys. **33**, 4149–4156 (2006).

[20]Y. Cui, J. G. Dy, B. Alexander, and S. Jiang, "Fluoroscopic gating without implanted fiducial markers for lung cancer radiotherapy based on support vector machines," Phys. Med. Biol. **53**, N315–N327 (2008).

[21]S. S. Korreman *et al.*, "The role of image guidance in respiratory gated radiotherapy," Acta Oncol. **47**, 1390–1396 (2008).

[22]J. Cai *et al.*, "Effects of breathing variation on gating window internal target volume respiratory gated radiation therapy," Med. Phys. **37**, 3927–3934 (2010).

[23]R. E. Wurm *et al.*, "Image guided respiratory gated hypofractionated stereotactic body radiation therapy (H-SBRT) for liver tumors: Initial experience," Acta Oncol. **45**, 881–889 (2006).

[24]N. Koch *et al.*, "Evaluation of internal lung motion for respiratory-gated radiotherapy using MRI: Part I—Correlating internal lung motion with skin fiducial motion," Int. J. Radiat. Oncol., Biol., Phys. **60**, 1459–1472 (2004).

[25]N. M. Wink, M. Chao, J. Anthony, and L. Xing, "Individualized gating windows based on four-dimensional CT information for respiration-gated radiotherapy," Phys. Med. Biol. **53**, 165–175 (2008).

[26]W. C. Wu, C. L. Chan, Y. W. Wong, and J. P. Cuijpers, "A study on the

influence of breathing phases in intensity-modulated radiotherapy of lung tumours using four-dimensional CT," Br. J. Radiol. **83**, 252–256 (2010).
[27]K. Suga, Y. Kawakami, M. Zaki, T. Yamashita, K. Shumizu, and N. Matsunga, "Clinical utility of co-registered respiratory-gated ^{99m}Tc-Technegas/MAA SPECT_CT images in the assessment of regional lung functional impairment in patients with lung cancer," Eur. J. Nucl. Med. Mol. Imaging **31**, 1280–90 (2004).
[28]M. Oliver, R. Staruch, A. Gladwish, J. Craig, J. Chen, and E. Wong, "Monte Carlo dose calculation of segmental IMRT delivery to a moving phantom using dynamic MLC and gating log files," Phys. Med. Biol. **53**, N187–N196 (2008).
[29]H. Wu, G. C. Sharp, Q. Zhao, H. Shirato, and S. B. Jiang, "Statistical analysis and correlation discovery of tumor respiratory motion," Phys. Med. Biol. **52**, 4761–4774 (2007).
[30]H. Shirato, S. Shimizu, K. Kitamura, T. Nishioka, K. Kagei, S. Hashimoto, H. Aoyama, T. Kunieda, N. Shinohara, H. Dosaka-Akita, and K. Miyasaka, "Four-dimensional treatment planning and fluoroscopic real-time tumour tracking radiotherapy," Int. J. Radiat. Oncol., Biol., Phys. **48**, 1187–1195 (2000).
[31]H. Wu, G. C. Sharp, B. Salzberg, D. Kaeli, H. Shirato, and S. B. Jiang, "A finite state model for respiratory motion analysis in image guided radiation therapy," Phys. Med. Biol. **49**, 5357–5372 (2004).

JJCO Japanese Journal of Clinical Oncology

Jpn J Clin Oncol 2011;41(4)462–468
doi:10.1093/jjco/hyq231
Advance Access Publication 22 December 2010

Long-term Outcomes of Fractionated Stereotactic Radiotherapy for Intracranial Skull Base Benign Meningiomas in Single Institution

Shunsuke Onodera[1,*], Hidefumi Aoyama[1], Norio Katoh[1], Hiroshi Taguchi[1], Kouichi Yasuda[1], Daisuke Yoshida[1], Ken Surtherland[2], Ryusuke Suzuki[2], Masayori Ishikawa[2], Bengua Gerard[2], Shunsuke Terasaka[3] and Hiroki Shirato[2]

[1]Department of Radiation Medicine, Hokkaido University Graduate School of Medicine, [2]Department of Medical Physics, Hokkaido University Graduate School of Medicine and [3]Department of Neurosurgery, Hokkaido University Graduate School of Medicine, Sapporo, Japan

*For reprints and all correspondence: Shunsuke Onodera, Department of Radiation Medicine, Hokkaido University Graduate School of Medicine, North 15, West 7, Kita-ku, Sapporo 060-8638, Japan. E-mail: m950086@jasmine.ocn.ne.jp

Received May 6, 2010; accepted November 21, 2010

Objective: To investigate the outcome of linac-based fractionated stereotactic radiotherapy over the last 10 years for intracranial skull base benign meningiomas in patients who were inoperable, who had residual tumors with some components of high mitotic index after surgery and who experienced relapse of the tumor.

Methods: Twenty-seven patients with intracranial skull base benign meningiomas treated with fractionated stereotactic radiotherapy were retrospectively reviewed. Twenty-seven cases were diagnosed as benign meningiomas on pathological (17 cases) or radiological (10 cases) examination. The median follow-up time was 90 months after initial treatment and 63 months after fractionated stereotactic radiotherapy. The median biological equivalent dose calculated using an α/β ratio of 2.0 Gy was 82.0 Gy (range, 60–106 Gy).

Results: The 5-year overall survival was 95.7 (95% confidence interval: 87.3–100)% after initial treatment and 96.2 (88.8–100)% after fractionated stereotactic radiotherapy. The 5-year overall survival and local control rate of patients who received fractionated stereotactic radiotherapy alone were both 100%. The 5-year progression-free survival and local control rate after fractionated stereotactic radiotherapy were all 100% with a tumor volume of <9.1 cc and 68.2 (37.2–99.2) and 75.8 (45.2–100)% for the tumors 9.1 cc, respectively. The difference was significant in progression-free survival ($P = 0.022$) and local control rate ($P = 0.044$). The local control rate was significantly worse in patients who received fractionated stereotactic radiotherapy for relapsed tumors ($P = 0.01$). No late radiation damage was observed in the follow-up period.

Conclusions: The long-term outcome suggests that fractionated stereotactic radiotherapy is a safe and effective treatment for intracranial skull base benign meningioma, especially for those who have tumors <9.1 cc or would receive fractionated stereotactic radiotherapy with or without surgery as the initial treatment.

Key words: radiation therapy – meningioma – stereotactic – skull base – fractionation

INTRODUCTION

Radiotherapy is increasingly being used for the treatment of meningiomas after incomplete resection, after recurrence and when tumor histology is atypical or malignant (1,2). When meningiomas are located in the intracranial skull base region, tumor excision is frequently incomplete and even biopsy can be hazardous (1). Therefore, it is a matter of

debate whether the use of radiotherapy should be used when the residual tumor is still small as the primary treatment or should be reserved as a potential salvage treatment for the residual tumor enlarged (3).

Stereotactic radiosurgery (SRS) has been proven useful for reducing unnecessary irradiation to the normal tissue surrounding meningiomas and provides an excellent local control rate (LCR) for small to mid-size skull base meningiomas (3,4). Three-dimensional conformal radiotherapy (3D-CRT) and fractionated stereotactic radiotherapy (FSRT) are expected to be useful for further reducing the possibility of late adverse reactions, even for relatively large tumors (5,6). Although there were several precise reports from a few institutions about the long-term outcome after FSRT (5–8), we are still short of knowledge about the treatment results of FSRT with the median follow-up longer than 60 months for intracranial meningioma.

We began using FSRT 15 years ago for patients with intracranial skull base meningiomas, principally for patients who were inoperable, who had residual tumors with some components of high mitotic index or high MIB-1 index, who experienced relapse of the tumor. In this study, we retrospectively reviewed our long-term results for FSRT of intracranial skull base benign meningiomas in order to investigate the usefulness and prognostic factors of this treatment.

PATIENTS AND METHODS

Patients

The outcome of 27 patients with intracranial skull base benign meningiomas treated with FSRT at Hokkaido University Hospital between May 1994 and February 2009 was retrospectively reviewed. Our treatment policy was to apply FSRT principally for those patients with intracranial skull base meningiomas who were inoperable, who had residual tumors or who experienced relapse of the tumor.

The patients' characteristics are summarized in Table 1, which were classified by the treatment category. In our cases, diagnosis was based on pathological examinations in 17 patients and radiological characteristics in 10 patients. The tumor was located at lateral structures in 17 (anterior fossa in 2, middle-lateral sphenoid wing in 8 and cerebellopontine angle and posterior fossa in 7 patients) and at central structures in 10 patients (cavernous sinus and tuberculum sellae in all 10 patients). The median tumor volume was 9.1 (range: 1.1–86.1) cc in all benign meningiomas. The median tumor volume in the initial treatment group was smaller than that in the salvage treatment group (6.3 vs. 12.3 cc), but there was no significant difference statistically ($P = 0.139$; Mann–Whitney test).

In this study, 11 patients were treated with FSRT alone as the initial treatment: 1 after biopsy (Simpson's grade V) and 10 after radiological diagnosis. Radiotherapy was used as a part of the initial treatment after incomplete excision in 4 patients and as a salvage treatment for tumor recurrence after surgery in 12 patients. The number of surgical procedures before FSRT was 1, 2 and 3 in 10, 5 and 1 patients, respectively. Patients who received open biopsy or surgery were classified according to Simpson's grade (9). Simpson's grade II (complete removal and coagulation of dual attachment) and IV (subtotal resection) surgery before radiotherapy was performed in 1 and 15 patients, respectively. Only one patient received biopsy (Simpson's grade V).

Table 1. Patients' characteristics

Factors	Initial treatment group	Salvage treatment group	Total
Total	15	12	27
Diagnosis			
Pathological diagnosis	5	12	17
Radiological diagnosis	10	0	10
Sex			
Male	1	6	7
Female	14	6	20
Age			
Mean (range)	60.3 (18–78)	45.5 (14–72)	53.7 (14–78)
Tumor cite			
Lateral	11	6	17
Central	4	6	10
Gross tumor volume			
Median (range) (cc)	6.3 (1.1–58.9)	12.3 (2.5–86.1)	9.1 (1.1–86.1)
Simpson's grade			
I	0	0	0
II	0	1	1
III	0	0	0
IV	4	11	15
V	1	0	1
Radiotherapy alone	10	0	10

Radiation Therapy Method

The gross tumor volume (GTV) was taken as the gross tumor shown on computed tomography (CT) with or without magnetic resonance imaging (MRI). The clinical target volume (CTV) was equal to the GTV, post-operative tumor bed or both in this study. The planning target volume (PTV) was 2–3 mm geometric expansion of the CTV. In delineating GTV, MRI co-registered with CT was used in 18 recent patients, and only the CT information was used for the remaining 9 patients.

Treatment planning systems were Focus or Xio (CMS Japan, Japan). A dose calculation algorithm used for the skull base meningiomas was the Clarkson method or the

convolution method. Stereotactic radiotherapy was carried out by using a 6 or 10 MV linear accelerator (LINAC) (2100C: Varian, Palo Alto, CA, USA; EXL15DP: Mitsubishi, Japan) with an in-house developed LINAC-based SRT system. Three-dimensional non-coplanar, single isocenter and the technique using multileaf collimator (MLC) were used. Three to eight static non-coplanar ports with the conformal fields were used in general. The width of these leafs was 5–10 mm at the isocenter. The dose was prescribed at the isocenter and defined as 100% in the dose distribution profile. MLCs were opened to cover PTV by a 90–95% isodose shell. The maximum dose point was always situated near the isocenter with the dose <110% (Fig. 1).

Patients were fixed by using a thermo-plastic mask and a custom-made head rest system. The dose to the optic chiasm was limited to ≤46 Gy. The total dose was 48–54 Gy in 26 cases and 32 Gy in 1 case using 2.0 Gy as the daily dose. When these radiation schedules were converted into the biological equivalent dose (BED) using an α/β ratio of 2.0 Gy, the median BED dose was 82.0 Gy (range: 52–90 Gy).

Follow-up and Statistical Analyses

The median follow-up time was 90 months (range: 21–209 months) after initial treatment, surgery or FSRT. The median follow-up time was 63 months (range: 19–154 months) after FSRT. More than 70% of patients were followed longer than 36 months after FSRT. Patients were periodically monitored by physical as well as radiographic examination in Hokkaido University Hospital and related hospitals. Local tumor progression (PD) was scored when the maximum diameter of the tumor increased 2 mm or more and partial reaction was scored when the diameter decreased 2 mm or more. The LCR was defined as no change or decrease of the tumor volume in the anatomical region consistent with the PTV of the treatment planning image. When more than 80% of the relapsed tumor volume was outside of the PTV, the recurrence was defined as out of field (10). In-field (>95% of the relapsed tumor volume in the PTV), marginal (20–95% of the relapsed tumor volume in the PTV), and out-of-field (less than 20% of the relapsed tumor volume in the PTV) recurrence were defined in this study.

Statistical analyses were conducted by using commercially available software (SPSS v18; IBM Inc., Chicago, IL). The overall survival (OS) and LCR were calculated from the date of the initiation of radiotherapy using the Kaplan–Meier method, and statistical evaluations were carried out by the log-rank test.

RESULTS

The OS, progression-free survival (PFS) and LCR at 5 years after initial treatment were 95.7 [95% confidence interval (CI): 87.3–100], 91.6 (80.4–100) and 95.5 (86.9–100)%.

The OS, PFS and LCR at 5 years after FSRT were 96.2 (88.8–100), 84.6 (67.7–100) and 88.6 (72.9–100)%.

Partial response was achieved in two benign patients, and the other patients with local control experienced no change of tumor volume. Three (11%) patients experienced in-field recurrence. These tumors had received Simpson's grade IV surgical resection. One patient had progression disease out of irradiation field. The recurrent cases were observed at the posterior fossa (at 55 and 81 months) in two patients, and at the cavernous sinus and tuberculum (at 19 and at 27 months) in two patients. These four recurrent cases are summarized in Table 2. No marginal recurrence was observed.

Univariate analyses were performed on OS, PFS and LCR after FSRT for patients with benign meningioma (Table 3). The female patients had significantly better PFS ($P = 0.009$) and LCR ($P = 0.04$) than the male patients. The 5-year OS, PFS and LCR after FSRT were all 100% for the benign meningiomas with a tumor volume of <9.1 cc and these parameters were 91.7 (76.0–100), 68.2 (37.2–99.2) and 75.8 (45.2–100)% for the tumors >9.1 cc, respectively. The difference was significant in PFS ($P = 0.022$) and LCR ($P = 0.044$) (Fig. 2).

In this study, the 11 patients who received FSRT alone had 100% OS, 88.9% PFS and 100% LCR at 5 years, respectively. The OS, PFS and LCR of patients who received FSRT with or without surgery as the initial treatment ($n = 15$) were 100, 91.7 and 100%, whereas those of patients who received FSRT for relapse ($n = 12$) were 90.9, 68.2 and 68.2%, respectively. The LCR was significantly worse in patients who received FSRT for a relapsed tumor ($P = 0.01$). A higher biological radiation dose, BED, was paradoxically associated with a lower PFS and LCR. The median tumor volume was larger (11.0 vs. 6.7 cc) and the ratio of patients with relapsed tumor was higher (7/11 vs. 5/16) in the higher

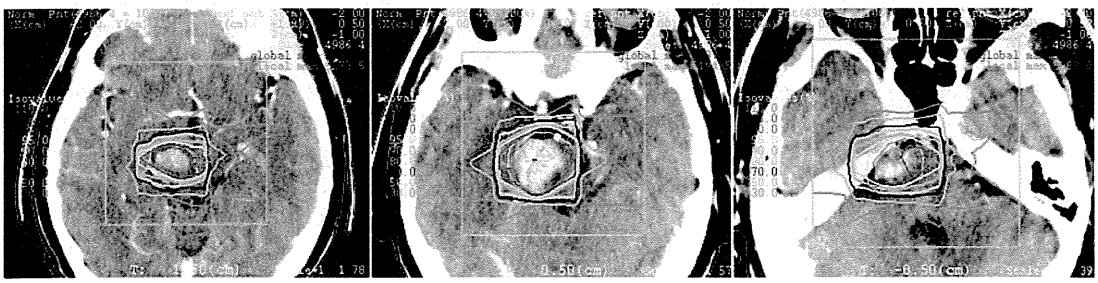

Figure 1. Dose distribution of FSRT for an intracranial benign meningioma. FSRT, fractionated stereotactic radiotherapy.

Table 2. The characteristics of patients with skull base benign meningioma who experienced tumor recurrence after FSRT either in-field or out-of-field

No.	Age	Sex	Primary site	Gross tumor volume (cc)	Simpson's grade	FSRT for relapsed tumor	Dose/fraction (Gy/fraction)	Local control	Recurrent site	Relapse (months)	Survival times	Final status
1	78	M	Cavernous sinus	58.9	Grade V	No	54 Gy/27fr	NC	Out-of-field	27	27	Alive
2	35	M	Cerebellopontine angle	9.75	Grade IV	Yes	54 Gy/27fr	PD	In-field	81	81	Alive
3	51	M	Cerebellopontine angle	13.9	Grade IV	Yes	44 Gy/ 22fr + 10 Gy/ 4fr	PD	In-field	55	55	Alive
4	58	F	Tuberculum sellae	24.9	Grade IV	Yes	54 Gy/27fr	PD	In-field	19	20	Death

FSRT, fractionated stereotactic radiotherapy; NC, no change; PD, progression of disease.

Table 3. The univariate analysis of prognostic factors after FSRT in patients with skull base benign meningiomas

Factor	5-year OS (95% CI)	*P* value	5-year PFS (95% CI)	*P* value	5-year LCR (95% CI)	*P* value
Age						
>60 ($n = 11$)	100	0.429	87.5 (64.6–100)	0.703	100	0.219
≤60 ($n = 16$)	93.8 (81.8–100)		82.0 (58.1–100)		82.0 (58.1–100)	
Gender						
Female ($n = 20$)	95.0 (85.4–100)	0.584	94.7 (84.7–100)	0.009	94.7 (84.7–100)	0.04
Male ($n = 7$)	100		55.6 (7.0–100)		66.7 (13.4–100)	
Gross tumor volume						
<9.1 cc ($n = 14$)	100	0.28	100	0.022	100	0.044
≥9.1 cc ($n = 13$)	91.7 (76.0–100)		68.2 (37.2–99.2)		75.8 (45.2–100)	
Planning method						
With MRI fusion ($n = 18$)	94.1(82.9–100)	0.467	86.5 (69.1–100)	0.229	93.8 (81.8–100)	0.473
Without MRI fusion ($n = 9$)	100		87.5 (64.6–100)		87.5 (64.6–100)	
Treatment for recurrence						
No ($n = 15$)	100	0.243	91.7 (76.0–100)	0.102	100	0.013
Yes ($n = 12$)	90.9 (73.8–100)		68.2 (27.6–100)		68.2 (27.6–100)	
Biological effective dose (Gy) ($\alpha/\beta = 2$)						
≥85 ($n = 11$)	90.9 (73.8–100)	0.243	60.6 (21.8–99.4)	0.006	68.2 (27.6–100)	0.013
<85 ($n = 16$)	100		100		100	

OS, overall survival; CI, confidence interval; PFS, progression-free survival; LCR, local control rate; MRI, magnetic resonance imaging.

dose group than the lower dose group, although the difference did not reach the level of statistical significance.

No adverse event was observed in the follow-up period. No optical injury, temporal lobe injury or hydrocephalus, or symptoms related to radiotherapy were observed.

DISCUSSION

The median dose used in the present study is 48–54 Gy with daily dose of 2.0 Gy. It is lower than the dose used in the Heiderberg study (5,7), in which the mean radiation dose was 56.8 Gy (±4.4 Gy), and higher than the dose used in the French study (8), in which 45 Gy with daily dose of 1.8 Gy was used. Since a dose–response curve for normal tissues and tumor changes rapidly at the dose range from 40 to 60 Gy with 1.8–2 Gy fractional dose, our results add new biological data for the meningioma and surrounding normal tissue with the long follow-up.

We found that the OS and LCR were 100% at 5 years after FSRT alone for patients with benign skull base meningioma who received FSRT as the initial treatment. This is consistent with a recent article by Korah et al. (6) in which the 8-year LCR was 94% after radiotherapy alone for

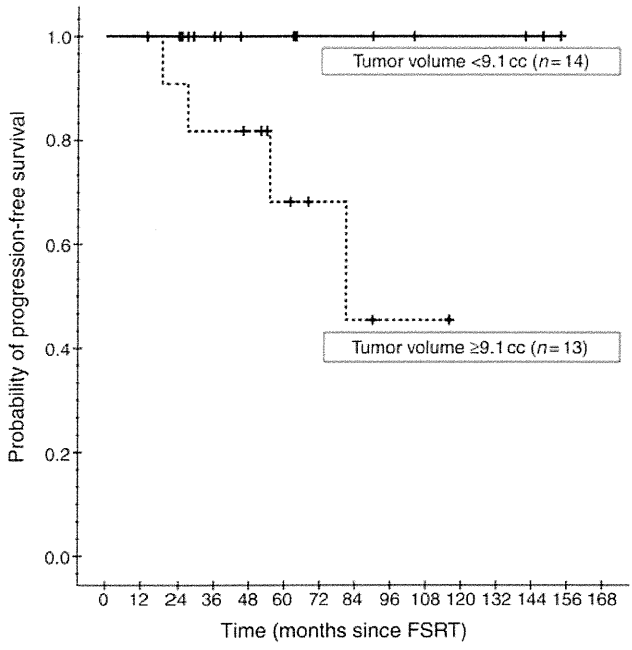

Figure 2. Progression-free survival curves according to the tumor volume. The patients were divided at a median volume of 9.1 cc.

42 patients. Lee et al. (10) also reported a 96.9% LCR at 5 years after SRS alone for 83 patients with cavernous sinus meningiomas. Other series have also suggested a high LCR after radiotherapy alone for benign meningiomas (4,5,11).

After incomplete surgical resection of Simpson's grade III or IV, the recurrence rate of meningiomas is high without radiotherapy (12,13). The recurrence rates for skull base meningioma are especially high, because total resection is much more difficult at this site than at other sites (12,14,15). Adjuvant FSRT immediately after subtotal resection has been suggested to reduce the recurrence rate without lowering the complication rate compared with previous radiotherapy (1,16,17). Previous reports have suggested that radiotherapy for recurrent meningioma is more difficult than radiotherapy used as the initial treatment (14,18). Condra et al. (1)reported that the cause-specific survival was better in patients who received radiotherapy immediately after subtotal resection than those who did not receive radiotherapy. Milker-Zabel et al. (5) also found that patients treated for recurrent meningioma showed a trend toward decreased PFS compared with patients treated with primary therapy, after biopsy or after subtotal resection ($P < 0.06$) in 179 patients with benign or atypical meningiomas.

Our results also suggested that better LCR were obtained for patients who received FSRT with or without surgery as the initial treatment than for those who received FSRT for relapsed tumors. However, the number of patients who were surgically treated and had residual tumor in our institution is uncertain. A small amount of residual benign meningioma after total or subtotal removal often does not enlarge or become symptomatic. Therefore, there is a possible bias that delayed irradiation was given for a poor prognosis group with a tendency of enlargement and irradiation was not required at all for the majority of patients in a good prognosis group. Precise selection criteria for the early irradiation after surgery are warranted to reduce the unnecessary irradiation for the good prognosis group.

The poorer outcome for recurrent meningioma is likely due to the progressive nature of some meningiomas or a mixed component of atypical meningioma (4,19,20). Meningiomas have been reported to obtain radioresistance or a component of malignant transformation as a natural course of the disease (20–23).

Considering that relapsed meningiomas often contain a progressive component, the treatment policy of applying radiotherapy only in the case of relapsed tumors causes a selection bias in the treatment outcome. The progressive nature of some meningiomas may also result in a leading bias with the treatment policy. Our study showed that the 5-year OS was 96.3% after any initial treatment and 88.2% after FSRT for the same patients' group. We summarized the previous studies of SRS and FSRT in Table 4 and found that our results contained the largest proportion of the relapsed tumors in these series. The tendency for the outcome to be better in the series with a lower proportion of relapsed tumors was not negligible. The lack of these biases may partly explain the excellent results in the group that received radiotherapy alone. The present study suggested that the selection bias and leading bias must be held in mind when we compare the treatment results of radiotherapy among different institutions or compare it with surgical series.

This study showed that the tumor volume was a significant prognostic factor as reported previously (5,22). We summarized the previous studies of SRS and FSRT which discriminated the tumor volume of benign tumors from atypical and malignant meningiomas (Table 4). The median tumor volume was 10 cc less in the majority of studies (4,10,11,24–29). The 5-year PFS and LCR values were more than 90% in these series. This study showed that our results of FSRT for tumors <9.1 cc (median) were as good as those in the previous studies. However, for the total patient group, including patients with larger tumors, the 5-year PFD and LCR were 84.6 and 88.6%, respectively. This finding is consistent with the results of Subach et al., who reported a mean tumor volume of 13.7 cc and a reduction of 5-year LCR to 86% (24).

Conventional 3D-CRT was reported to achieve excellent results in 1980s–early 1990s when CT and MRI images had 5 mm slice thickness and very precise fixation did not make sense. However, in the late 1990s, treatment planning using images with 1–2 mm thickness began to require precise fixation of the skull. Although there is no randomized studies to compare 3D-CRT and FSRT, FSRT can reduce the dose to the critical part of brain tissue with higher certainty than conventional 3D-CRT in the era of 1–2 mm slice thickness of the medical images. There are two recent reviews comparing different radiotherapy techniques such as 3D-CRT, SRS

Table 4. Previous studies of stereotactic radiosurgery and fractionated stereotactic radiotherapy for skull base benign meningioma in which the median or mean tumor volume was described for benign tumors

Institution	SRS or FSRT	No. of patients	Tumor volume median (range) (cc)	Recurrent cases (%)	Follow-up period median (range) (months)	PFS	LCR
Mayo Clinic (30)	SRS	88	10 (2.3–30)	>3 (3%)	35 (12–83)	95.0%	—
University of Pittsburgh (24)	SRS	60	13.7[a] (0.8–56.8)	>13 (21%)	35[a] (12–101)	—	86.7%
University of Pittsburgh (10)	SRS	155	6.5 (0.5–52.4)	Unknown	39[a] (2–145)	—	93.1%
University Hospital, Verona (25)	SRS	111	8.1[a] (1–20)	0 (0%)	48.2 (12.1–82.5)	96.0%	97.0%
CHU La Timone (4)	SRS	32	2.28[a] (0.25–60)	2 (6%)	56[a] (24–118)	100.0%	—
University of Pittsburgh (26)	SRS	219	5.0 (0.47–56.5)	0 (0%)	29 (2–164)	—	93%
Medical University Graz (28)	SRS	200	6.5 (0.38–89.8)	Unknown	94.8 (60–144)	98.5%	—
Seoul National University (11)	SRS	63	6.3[a] (0.5–18.4)	1 (2%)	77[a] (48–112)	90.2%	—
University of Pittsburgh (29)	SRS	168	6.1 (0.3–32.5)	35 (21%)	72 (–254)	91.0%	97% (at 10 years)
University of California (27)	FSRT	45	14.5 (1.4–65.66)	8 (31%)	36 (12–53)	97.4% (3 years)	—
Hokkaido University (9.1 cc>)	FSRT	14	4.7 (1.1–9.0)	4 (28.6%)	79.0 (27–154)	100.0%	100.0%
Hokkaido University (all cases)	FSRT	27	9.1 (1.1–86.1)	12 (44.4%)	63.0 (19–154)	84.6%	88.6%

SRS, stereotactic radiosurgery.
[a]Mean.

and FSRT (30,31). Elia et al. (30) summarized that FSRT has toxicity equivalent to that of SRS, despite its biased use for larger meningiomas with more complicated volumes. Minniti et al. (31) recommended SRS only for tumors <3 cm away more than 3 mm from the optic pathway because of the high risk of long-term neurological deficits.

Selch et al. (27) reported an encouraging 3-year PFS of 97% after FSRT for patients with a median tumor volume of 14.5 cc using a dose fractionation schedule similar to that in our study. Milker-Zabel et al. (5) have published results of FSRT for 179 skull base meningiomas, achieving 90.5 and 89% recurrence-free survival rates for benign meningiomas and atypical meningiomas, respectively, and using a median dose of 57.6 Gy (range: 45–68 Gy). Their results were excellent considering that the median target volume was as large as 33.6 cm^3 (1–412.6 cm^3) and as many as 141 (44.5%) cases of recurrent disease were included. Eight (4.4%) patients developed new clinical symptoms, such as reduced vision, trigeminal neuralgia and intermittent tinnitus located at the side of the irradiated meningioma after FSRT in their series. The slightly higher dose used in their study might have been the reason for the better tumor control with a little higher complication rate compared with our study. Korah et al. (6) used FSRT, 3D-CRT and SRS for 9, 11 and 22 patients, respectively, and among these, only 1 patient treated with SRS developed a symptomatic radiation-related neurological complication. There were no late adverse reactions in our series (27). Considering that a lower complication rate is an extremely important issue for patients with benign tumors, FSRT is one of the initial treatment options for patients with intracranial skull base meningioma which locate very close to the critical portion of normal brain tissues.

However, in our relapse cases, the LCR was low. We consider that the 2–3 mm PTV margin was sufficient with our FSRT technique by adding MLC margin to cover the PTV with 90–95% isodose line. However, it is not deniable that the high relapse rate of the larger tumors may also be explained by the small PTV margins used in our study. Goldsmith et al. (32) reported that the PFS rate in the group treated with a minimum tumor dose of >52 Gy was better than the group treated with ≤52 Gy (93 vs. 65%; $P = 0.04$). When FSRT was used for treating the case of the tumor located near the organ at risk (OAR), we must have reduced the margin for PTV to exclude the OAR from the high-dose area. Thus, the dose concentration for the tumor was gotten worse than an ideal dose distribution. Intensity-modulated radiotherapy (IMRT) is expected to increase the therapeutic ratio by reducing the dose to normal tissue because IMRT can deliver the prescription dose to the targets without worsen the dose concentration. For improvement of the LCR of those relapse cases, IMRT with a fractionated schedule will be more appropriate than simple FSRT to increase the dose for these tumors without increasing the dose to the surrounding normal tissue (33–36). However, higher radiation dose to the rest of the body and higher cost to the patient must be taken into account for each patient to use IMRT.

In conclusion, the long-term outcome suggests that FSRT is a safe and effective treatment for intracranial skull base benign meningioma, especially for those who have tumors <9.1 cc or would receive FSRT with or without surgery as the initial treatment.

Funding

This study was partly supported by Grant-in-Aid for Scientific Research (no. 21249065) from Ministry of Education, Culture, Sports, Science and Technology, Japan, and a part of this study was presented in the poster session of 51th Annual Meeting of ASTRO in Chicago (USA), 1–5 November 2009.

Conflict of interest statement

None declared.

References

1. Condra KS, Buatti JM, Mendenhall WM, Friedman WA, Marcus RB, Jr, Rhoton AL. Benign meningiomas: primary treatment selection affects survival. *Int J Radiat Oncol Biol Phys* 1997;39:427–36.
2. Whittle IR, Smith C, Navoo P, Collie D. Meningiomas. *Lancet* 2004;363:1535–43.
3. Kondziolka D, Flickinger JC, Perez B. Judicious resection and/or radiosurgery for parasagittal meningiomas: outcomes from a multicenter review. Gamma Knife Meningioma Study Group. *Neurosurgery* 1998;43:405–13; discussion 13–4.
4. Roche PH, Pellet W, Fuentes S, Thomassin JM, Regis J. Gamma knife radiosurgical management of petroclival meningiomas results and indications. *Acta Neurochir (Wien)* 2003;145:883–8; discussion 8.
5. Milker-Zabel S, Zabel A, Schulz-Ertner D, Schlegel W, Wannenmacher M, Debus J. Fractionated stereotactic radiotherapy in patients with benign or atypical intracranial meningioma: long-term experience and prognostic factors. *Int J Radiat Oncol Biol Phys* 2005;61:809–16.
6. Korah MP, Nowlan AW, Johnstone PA, Crocker IR. Radiation therapy alone for imaging-defined meningiomas. *Int J Radiat Oncol Biol Phys* 2010;76:181–6.
7. Milker-Zabel S, Zabel-du Bois A, Huber P, Schlegel W, Debus J. Fractionated stereotactic radiation therapy in the management of benign cavernous sinus meningiomas : long-term experience and review of the literature. *Strahlenther Onkol* 2006;182:635–40.
8. Litre CF, Colin P, Noudel R, Peruzzi P, Bazin A, Sherpereel B, et al. Fractionated stereotactic radiotherapy treatment of cavernous sinus meningiomas: a study of 100 cases. *Int J Radiat Oncol Biol Phys* 2009;74:1012–7.
9. Simpson D. The recurrence of intracranial meningiomas after surgical treatment. *J Neurol Neurosurg Psychiatry* 1957;20:22–39.
10. Lee JY, Niranjan A, McInerney J, Kondziolka D, Flickinger JC, Lunsford LD. Stereotactic radiosurgery providing long-term tumor control of cavernous sinus meningiomas. *J Neurosurg* 2002;97:65–72.
11. Han JH, Kim DG, Chung HT, Park CK, Paek SH, Kim CY, et al. Gamma knife radiosurgery for skull base meningiomas: long-term radiologic and clinical outcome. *Int J Radiat Oncol Biol Phys* 2008;72:1324–32.
12. De Jesus O, Sekhar LN, Parikh HK, Wright DC, Wagner DP. Long-term follow-up of patients with meningiomas involving the cavernous sinus: recurrence, progression, and quality of life. *Neurosurgery* 1996;39:915–9; discussion 9–20.
13. Mathiesen T, Lindquist C, Kihlstrom L, Karlsson B. Recurrence of cranial base meningiomas. *Neurosurgery* 1996;39:2–7; discussion 8–9.
14. Maroon JC, Kennerdell JS, Vidovich DV, Abla A, Sternau L. Recurrent spheno-orbital meningioma. *J Neurosurg* 1994;80:202–8.
15. Black PM, Villavicencio AT, Rhouddou C, Loeffler JS. Aggressive surgery and focal radiation in the management of meningiomas of the skull base: preservation of function with maintenance of local control. *Acta Neurochir (Wien)* 2001;143:555–62.
16. Debus J, Wuendrich M, Pirzkall A, Hoess A, Schlegel W, Zuna I, et al. High efficacy of fractionated stereotactic radiotherapy of large base-of-skull meningiomas: long-term results. *J Clin Oncol* 2001;19:3547–53.
17. Mendenhall WM, Morris CG, Amdur RJ, Foote KD, Friedman WA. Radiotherapy alone or after subtotal resection for benign skull base meningiomas. *Cancer* 2003;98:1473–82.
18. Al-Mefty O, Kadri P, Pravdenkova S, Sawyer JR, Stangeby C, Husain M. Malignant progression in meningioma: documentation of a series and analysis of cytogenetic findings. *J Neurosurg* 2004;101:210–8.
19. Aghi MK, Carter BS, Cosgrove GR, Ojemann RG, Amin-Hanjani S, Martuza RL, et al. Long-term recurrence rates of atypical meningiomas after gross total resection with or without postoperative adjuvant radiation. *Neurosurgery* 2009;64:56–60.
20. Ohba S, Yoshida K, Hirose Y, Ikeda E, Kawase T. Early malignant transformation of a petroclival meningothelial meningioma. *Neurosurg Rev* 2009;32:495–9.
21. Colvett KT, Hsu DW, Su M, Lingood RM, Pardo FS. High PCNA index in meningiomas resistant to radiation therapy. *Int J Radiat Oncol Biol Phys* 1997;38:463–8.
22. Maillo A, Orfao A, Espinosa AB, Sayagues JM, Merino M, Sousa P, et al. Early recurrences in histologically benign/grade I meningiomas are associated with large tumors and coexistence of monosomy 14 and del(1p36) in the ancestral tumor cell clone. *Neuro Oncol* 2007;9:438–46.
23. Nakane Y, Natsume A, Wakabayashi T, Oi S, Ito M, Inao S, et al. Malignant transformation-related genes in meningiomas: allelic loss on 1p36 and methylation status of p73 and RASSF1A. *J Neurosurg* 2007;107:398–404.
24. Subach BR, Lunsford LD, Kondziolka D, Maitz AH, Flickinger JC. Management of petroclival meningiomas by stereotactic radiosurgery. *Neurosurgery* 1998;42:437–43; discussion 43–5.
25. Nicolato A, Foroni R, Alessandrini F, Maluta S, Bricolo A, Gerosa M. The role of Gamma Knife radiosurgery in the management of cavernous sinus meningiomas. *Int J Radiat Oncol Biol Phys* 2002;53:992–1000.
26. Flickinger JC, Kondziolka D, Maitz AH, Lunsford LD. Gamma knife radiosurgery of imaging-diagnosed intracranial meningioma. *Int J Radiat Oncol Biol Phys* 2003;56:801–6.
27. Selch MT, Ahn E, Laskari A, Lee SP, Agazaryan N, Solberg TD, et al. Stereotactic radiotherapy for treatment of cavernous sinus meningiomas. *Int J Radiat Oncol Biol Phys* 2004;59:101–11.
28. Kreil W, Luggin J, Fuchs I, Weigl V, Eustacchio S, Papaefthymiou G. Long term experience of gamma knife radiosurgery for benign skull base meningiomas. *J Neurol Neurosurg Psychiatry* 2005;76:1425–30.
29. Flannery TJ, Kano H, Lunsford LD, Sirin S, Tormenti M, Niranjan A, et al. Long-term control of petroclival meningiomas through radiosurgery. *J Neurosurg* 2010;112:957–64.
30. Elia AEH, Shih HA, Loeffler JS. Stereotactic radiation treatment for benign meningiomas. *Neurosurg Focus* 2007;23:E5.
31. Minniti G, Amichetti M, Enrici RM. Radiotherapy and radiosurgery for benign skull base meningiomas. *Radiat Oncol* 2009;4:42.
32. Goldsmith BJ, Wara WM, Wilson CB, Larson DA. Postoperative irradiation for subtotally resected meningiomas. A retrospective analysis of 140 patients treated from 1967 to 1990. *J Neurosurg* 1994;80:195–201.
33. Khoo VS, Oldham M, Adams EJ, Bedford JL, Webb S, Brada M. Comparison of intensity-modulated tomotherapy with stereotactically guided conformal radiotherapy for brain tumors. *Int J Radiat Oncol Biol Phys* 1999;45:415–25.
34. Pirzkall A, Carol M, Lohr F, Hoss A, Wannenmacher M, Debus J. Comparison of intensity-modulated radiotherapy with conventional conformal radiotherapy for complex-shaped tumors. *Int J Radiat Oncol Biol Phys* 2000;48:1371–80.
35. Pirzkall A, Debus J, Haering P, Rhein B, Grosser KH, Hoss A, et al. Intensity modulated radiotherapy (IMRT) for recurrent, residual, or untreated skull-base meningiomas: preliminary clinical experience. *Int J Radiat Oncol Biol Phys* 2003;55:362–72.
36. Milker-Zabel S, Zabel-du Bois A, Huber P, Schlegel W, Debus J. Intensity-modulated radiotherapy for complex-shaped meningioma of the skull base: long-term experience of a single institution. *Int J Radiat Oncol Biol Phys* 2007;68:858–63.

JOURNAL OF APPLIED CLINICAL MEDICAL PHYSICS, VOLUME 12, NUMBER 3, SUMMER 2011

Detection of patient setup errors with a portal image – DRR registration software application

Kenneth Sutherland,[1a] Masayori Ishikawa,[1] Gerard Bengua,[2] Yoichi M. Ito,[1] Yoshiko Miyamoto,[1] and Hiroki Shirato[1,2]
Hokkaido University Graduate School of Medicine,[1] Sapporo 060-8648, Japan; Hokkaido University Hospital,[2] Sapporo 060-8648, Japan
kensuth@med.hokudai.ac.jp

Received 25 October, 2010; accepted 13 February, 2011

The purpose of this study was to evaluate a custom portal image — digitally reconstructed radiograph (DRR) registration software application. The software works by transforming the portal image into the coordinate space of the DRR image using three control points placed on each image by the user, and displaying the fused image. In order to test statistically that the software actually improves setup error estimation, an intra- and interobserver phantom study was performed. Portal images of anthropomorphic thoracic and pelvis phantoms with virtually placed irradiation fields at known setup errors were prepared. A group of five doctors was first asked to estimate the setup errors by examining the portal and DRR image side-by-side, not using the software. A second group of four technicians then estimated the same set of images using the registration software. These two groups of human subjects were then compared with an auto-registration feature of the software, which is based on the mutual information between the portal and DRR images. For the thoracic case, the average distance between the actual setup error and the estimated error was 4.3 ± 3.0 mm for doctors using the side-by-side method, 2.1 ± 2.4 mm for technicians using the registration method, and 0.8 ± 0.4 mm for the automatic algorithm. For the pelvis case, the average distance between the actual setup error and estimated error was 2.0 ± 0.5 mm for the doctors using the side-by-side method, 2.5 ± 0.4 mm for technicians using the registration method, and 2.0 ± 1.0 mm for the automatic algorithm. The ability of humans to estimate offset values improved statistically using our software for the chest phantom that we tested. Setup error estimation was further improved using our automatic error estimation algorithm. Estimations were not statistically different for the pelvis case. Consistency improved using the software for both the chest and pelvis phantoms. We also tested the automatic algorithm with a database of over 5,000 clinical cases from our hospital. The algorithm performed well for head and breast but performed poorly for pelvis cases, probably due to lack of contrast in the megavoltage portal image. The software incorporates an original algorithm to fuse portal and DRR images, which we describe in detail. The offset optimization algorithm used in the automatic mode of operation is also unique, and may be useful if the contrast of the portal images can be improved.

PACS numbers: 87.55.Qr, 87.57.nj

Key words: patient setup, image registration, portal imaging, mutual information

[a] Corresponding author: Kenneth Sutherland, Hokkaido University Graduate School of Medicine, Sapporo-shi Kita-ku Kita 14 Jo Nishi 5 Chome, 060-8648 Japan; phone:+81-11-706-7638; fax:+81-11-706-7639; email: kensuth@med.hokudai.ac.jp

I. INTRODUCTION

Traditionally doctors have judged patient setup errors by viewing portal images alongside planning digital reconstructed radiograph (DRR) images, either with paper printouts, films on a light board, or on a computer terminal. Estimation of the error is made by measuring the distance from the isocenter to anatomical structures (usually bones) visible in both images.[1] However, the process is often inaccurate, with errors between 5 and 10 mm being reported.[2]

Fully and semi-automatic methods based on electronic portal imaging devices (EPIDs),[3] implanted fiducial surrogate markers imaged with kilovoltage fluoroscopy,[4] on-board imager (OBI, Varian Medical Systems, Palo Alto, CA)[5] and cone-beam CT (CBCT), have recently become common. However, these methods often require additional cost, exposure of X-rays, and longer time for setup. As a result, for a large number of patients who do not require a high accuracy of patient positioning (e.g., palliative treatments or mantle field radiation), portal imaging once or twice during the first week of treatment is still desirable.

The standard patient treatment regime employed at our institution involves first obtaining a CT scan of the patient which will be used for treatment planning. A DRR reconstruction of the beam's eye view (BEV) is computed and stored by a commercial treatment planning system (TPS). The treatment port, isocenter, orthogonal axes with scale information (a tick mark each centimeter) and other treatment information are burned into the DRR image.

Portal images are usually obtained at our hospital before the first treatment fraction using a megavoltage X-ray source from a linear accelerator and a computed radiograph (CR) system (Fuji Medical Co., Ltd., Tokyo, Japan). Images are captured onto photosensitive plates, which are scanned to produce high resolution (usually 1760×1760 pixels) deep bit (10 bits per pixel) images. The portal images also contain scale information on the orthogonal axes with a small dot each centimeter. The portal and DRR images are compared to determine that the treatment beam accurately targets the planned treatment volume (PTV) while avoiding organs at risk (OARs). If a problem is detected, the presiding physician may request that the couch position be adjusted. Portal images are then retaken and rechecked against the DRR.

We developed an image registration software application for the estimation of patient setup error. DRRs from any commercial TPS can be opened using common file formats (e.g., bitmap, JPEG, DICOM). The software works for any anatomical region or gantry angle. The software can be operated manually, or with an automatic registration mode based on the mutual information between the images.

The purpose of this study is to verify that our software actually improves setup error detection compared with the traditional side-by-side method. There is little statistical evidence in the literature of the superiority of image registration to side-by-side human estimation of setup error from two-dimensional portal images. We evaluated the efficacy of the software as an aid for the clinical staff to improve setup accuracy using a prospective phantom study and its statistical analysis. We compared the ability of humans to correctly determine a known setup error with and without the software. An automatic mode of operation of the software was also tested with a database of clinical cases, collected over several years, for which the setup up error was determined by the consensus of a trained software operator (medical physicist), a radiation technician and the presiding oncologist.

II. MATERIALS AND METHODS

A. Patient setup error detection software

After a CT scan of the patient is obtained, a DRR of the BEV is computed and stored with a TPS. The treatment port, isocenter, orthogonal axes with scale information (a tick mark each centimeter) and other treatment information are burned into the image. The DRR image is

saved in a database accessible to our software. Portal images are usually obtained before the first treatment fraction using a double exposure (open field and the actual field) with a megavoltage X-ray source from a linear accelerator, captured with a CR system. The portal images also contain graphical scale information on the orthogonal axes with a small dot or tick mark every centimeter from the isocenter.

In our proposed method, while the patient is lying on the treatment couch, the planning DRR and portal images are loaded into the software. The isocenter and two points on orthogonal axes, usually 10 cm from the isocenter, are designated by clicking on the images with the mouse. The locations of the points are determined by the operator using the axis and scale tick marks on each image. The software uses the three control points to determine scaling and rotation in order to transform the portal image into the coordinate space of the DRR image. Because the imaging plate may not be exactly orthogonal to the beam axis, especially when an oblique gantry angle is used, the portal image may be warped. The software can correct for these out-of-plane rotations.

After the images have been successfully fused, the operator uses bony landmarks or other visible anatomical features in order to determine setup error. The portal image can be shifted horizontally or vertically and rotated clockwise or counterclockwise relative to the stationary DRR image. An example screenshot is shown in Fig. 1.

The operator can apply complementary colors, such as red and cyan, to make the fused image more distinguishable. If the images align exactly, each resulting pixel will be a level of grey. Misalignments are visible as color shadows. The operator can specify which pair of complementary colors to apply, depending on which colors are easier to see. Brightness and contrast can also be adjusted on both images to make bony features more distinguishable. The user can also rapidly flip between the DRR, portal and fused images. After the images are successfully registered, the treatment field shift (in mm) and rotation (in degrees), corresponding to the BEV, is displayed. The required couch movement to correct the offset, based on the gantry angle, can also be computed and displayed.

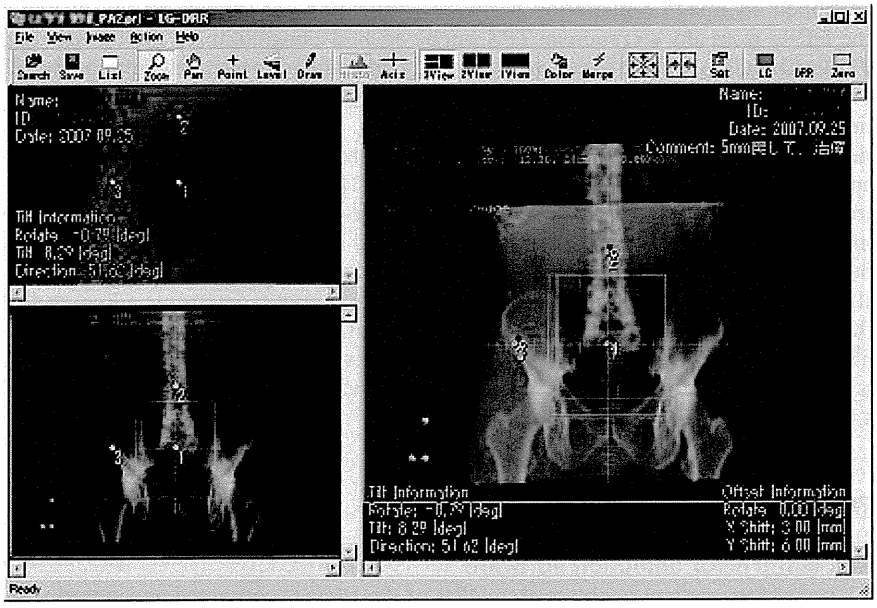

FIG. 1. The Portal-DRR software. The user specifies three points on the portal (top left) and DRR (bottom left) images using grid spacing tick marks.The merged image (right) is used to compare internal bony structures in order to determine the setup error, which is displayed at the lower right.

B. Theory of image distortion correction

Distortions of portal images may include rotations about the beam axis (z-axis) and rotations about an axis perpendicular to the beam axis (x- or y-axis). It is difficult to independently correct rotations about the x and y axes. We therefore devised a scheme to treat rotations about the x and y axes as equivalent rotations about an arbitrary axis perpendicular to the z-axis, denoted as the x'-axis. The x'-axis lies in the x, y plane and points in the direction of the tilt. It is possible to compose rotations about the x'-axis from equivalent rotations about the x and y axes, combined with a rotation about the z-axis. Coordinates on the imaging plate (x', y') correspond to the original coordinates (x, y) as follows:

$$\begin{pmatrix} x' \\ y' \end{pmatrix} = b \cdot Rot(\theta) \cdot Rot(\varphi) \cdot St(\phi) \cdot Rot^{-1}(\varphi) \begin{pmatrix} x \\ y \end{pmatrix} \tag{1}$$

Here b is the zoom ratio, $Rot(\theta)$ is the rotation about the z-axis, Rot(ϕ) is the rotation about the x'-axis, and St(Θ) is the stretch ratio produced by the rotation about the x-axis. The rotation and stretch functions are defined as:

$$\text{Rot}(\theta) = \begin{pmatrix} \cos\theta & -\sin\theta \\ \sin\theta & \cos\theta \end{pmatrix}, St(\phi) = \begin{pmatrix} 1 & 0 \\ 0 & \dfrac{1}{\cos\phi} \end{pmatrix} \tag{2}$$

One can obtain the original image pixel coordinates by applying the reverse process in order to correct the distorted image:

$$\begin{pmatrix} x \\ y \end{pmatrix} = \frac{1}{b} \cdot Rot(\varphi) \cdot St^{-1}(\phi) \cdot Rot^{-1}(\varphi) \cdot Rot^{-1}(\theta) \begin{pmatrix} x' \\ y' \end{pmatrix} \tag{3}$$

Because parameters θ, ϕ, and Θ can be obtained from two arbitrary coordinates, according to the equations, we can proceed as follows.

$$\begin{aligned} \varphi &= \arctan\left(\frac{1}{2}\left(\alpha + \sqrt{4+\alpha^2}\right)\right) \qquad \varphi + \theta = arctan\left(\frac{m\cos\varphi + n\sin\varphi}{k\cos\varphi + l\sin\varphi}\right) \\ \phi &= \cos^{-1}\left(\frac{m\cos\varphi + n\sin\varphi}{k\sin\varphi - l\cos\varphi}\right) \qquad b = \frac{\cos(\varphi+\theta)}{k\cos\varphi + l\sin\varphi} \end{aligned} \tag{4}$$

Note that k, l, m and n are in the original beam axis' coordinate system and can be computed from two pairs of points.

$$\begin{pmatrix} k & l \\ m & n \end{pmatrix} = \begin{pmatrix} x_1 & x_2 \\ y_1 & y_2 \end{pmatrix} \begin{pmatrix} x'_1 & x'_2 \\ y'_1 & y'_2 \end{pmatrix}^{-1} = \frac{1}{x'_1 y'_2 - x'_2 y'_1} \cdot \begin{pmatrix} x_1x'_1 + x_2y'_1 & x_1x'_2 + x_2y'_2 \\ y_1x'_1 + y_2y'_1 & y_1x'_2 + y_2y'_2 \end{pmatrix} \tag{5}$$

The conversion process is illustrated in Fig. 2.

The proposed image-registration method uses imaging plates to obtain portal images for irradiation field verification. For non-zero gantry angles, the imaging plate is held freely on a stand without fixation to a certain coordinate system. In order to correct perspective distortion due to the imaging plate not being orthogonal to the beam axis, three control points are

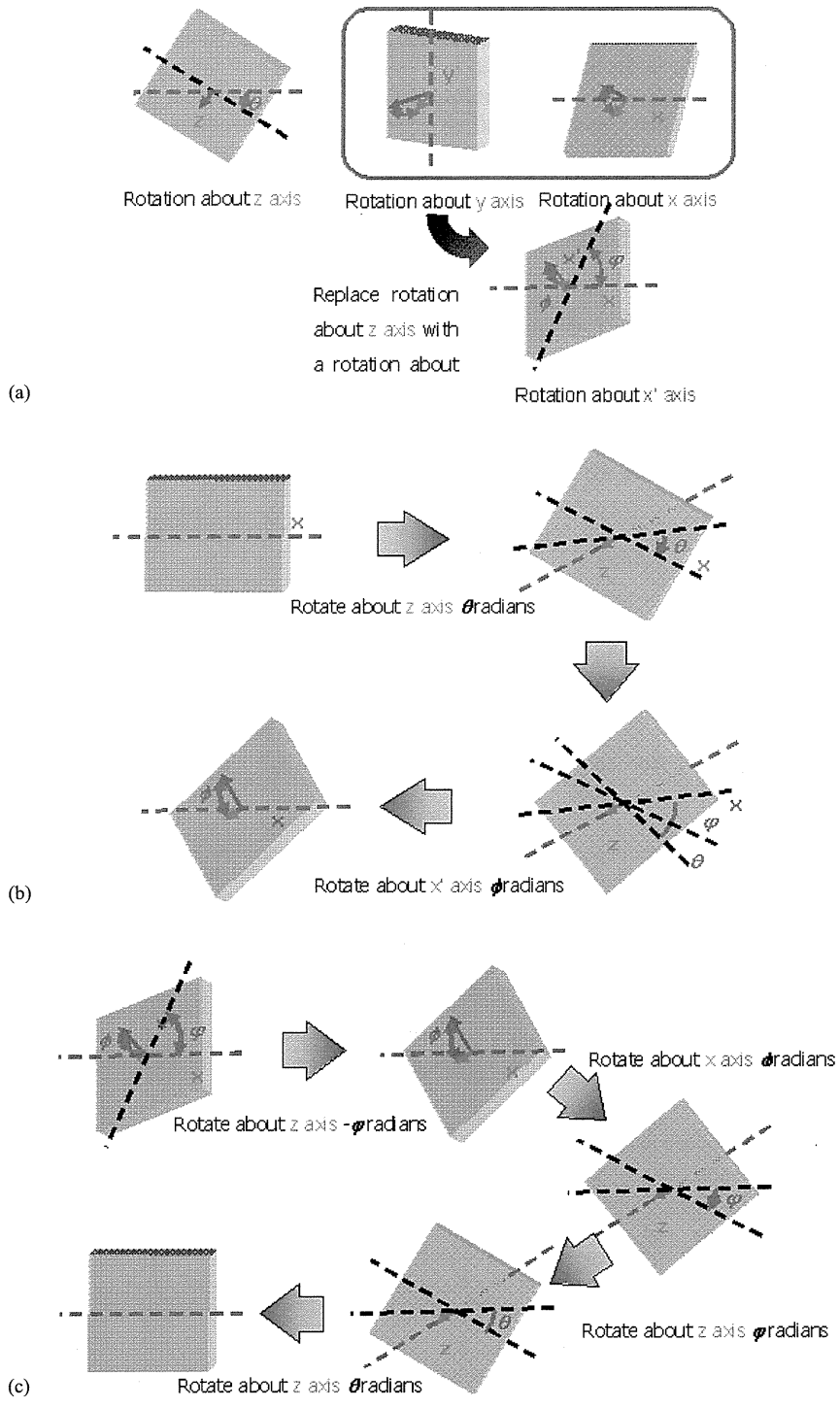

FIG. 2. Conversion of rotation axis for image distortion.

manually placed using graphical axis scale tick marks on each image. The specified points should cover the area of the image containing bony structures used for alignment. We refer to the area roughly surrounding the control points as the "working area".

To test the correction function, an electronic tiltmeter was used to measure a 10° tilt of the imaging plate about the horizontal axis. The plate was exposed to X-rays using the linac axis grid. The resulting image was fused with a dummy DRR image. A test point was placed at a position 5 cm along the x- and y-axis within the working area. The distance from the test point on the DRR image and the transformed portal image point was measured. The experiment was repeated with the test point outside the working area. The experimental setup is illustrated in Fig. 3.

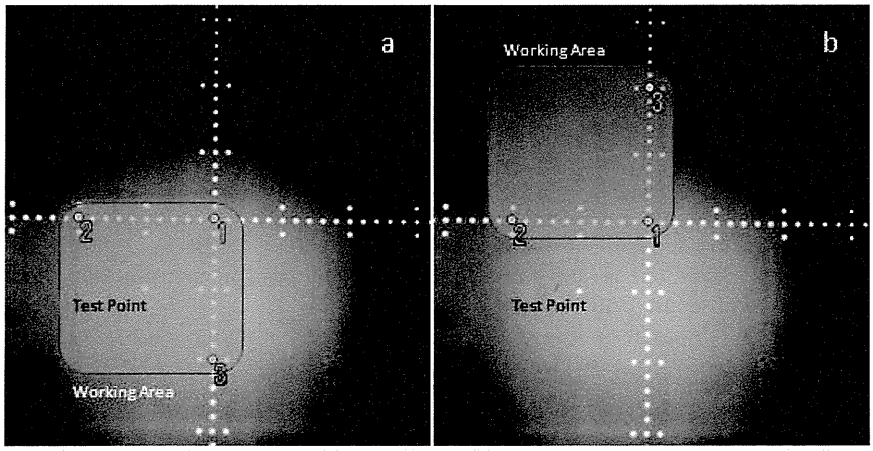

FIG. 3. Tilt experiment setup. The imaging plate was tilted 10° horizontally. The test point (5 cm along the x- and y-axis) was inside the working area for (a) and outside the working area for (b). The test point was transformed into the DRR image coordinates and the distance from the corresponding point specified on the DRR image was measured.

C. Automatic determination of patient setup error

We developed a method to automatically determine the x-y shift and in-plane rotation based on the mutual information (MI) of the pixel intensity values of the overlapping portions of the transformed portal and DRR images. The entropy of a single image can be computed from the equation:

$$H = \sum_i p_i \cdot \log \frac{1}{p_i} \tag{6}$$

where p_i is the probability of a gray-level pixel value i estimated from the histogram of the image.[6] The joint entropy between two images can likewise be defined as:

$$H(A,B) = -\sum_{i,j} p(i,j) \cdot \log[p(i,j)] \tag{7}$$

where $p(ij)$ is the probability of gray-level pixel value i from one image (A) and the gray-level pixel value j from the second image (B) at the same position. Mutual information is then defined as:

$$I(A,B) = H(A) + H(B) - H(A,B) \tag{8}$$